PAPER

Nonlinear structures of traveling waves in the cubic–quintic complex Ginzburg–Landau equation on a finite domain

Phys. Scr. **87** (2013) 065001 (8pp) doi:10.1088/0031-8949/87/06/065001

Nonlinear structures of traveling waves in the cubic–quintic complex Ginzburg–Landau equation on a finite domain

J B Gonpe Tafo[1], L Nana[2] and T C Kofane[1,3]

[1] Laboratoire de Mécanique, Département de Physique, Faculté des Sciences, Université de Yaoundé I, PB 812, Yaoundé, Cameroun
[2] Laboratoire de Physique Fondamentale, Groupe Phénomènes Non Linéaires et Systèmes Complexes, UFD de Mathématique, Informatique Appliquée et Physique Fondamentale, Université de Douala, PB 24157, Douala, Cameroun
[3] The Abdus Salam International Center for Theoretical Physics, PO Box 586, Strada Costiera 11, I-34014 Trieste, Italy

E-mail: joelgbruno@yahoo.fr, la_-nanad@yahoo.fr and tckofane@yahoo.com

Received 8 October 2012
Accepted for publication 5 April 2013
Published 3 May 2013
Online at stacks.iop.org/PhysScr/87/065001

Abstract
We investigate the behavior of traveling waves in a spatial domain with the homogeneous boundary conditions by using the one-dimensional cubic–quintic complex Ginzburg–Landau equation. We focus our work on the absolute and convective instabilities and determine the dynamical regimes that are observed. As a consequence in the convectively unstable regime, the waves ultimately decay at any fixed position. Only when the threshold for the absolute instability is exceeded, the wave patterns may be maintained against the dissipation at the boundary. Consequently, coherent structures may be observed in the last case. We build a new state of phase diagram in the parameter plane spanned by the criticality parameter and the quintic nonlinear coefficient.

PACS numbers: 05.45.−a, 47.54.+r

(Some figures may appear in colour only in the online journal)

1. Introduction

Several physico-chemical systems driven out of equilibrium present oscillatory instabilities corresponding to the Hopf bifurcations [1]. Close to such instabilities, the dynamics of the system are usually reduced to amplitude equations of the complex Ginzburg–Landau type, which describe the evolution of the patterns that appear beyond the bifurcation point [2]. One of the main sources of richness in wave patterns is the existence of two regimes of instability: the convective instability and the absolute one [3]. This distinction arises when the group velocity of the wave is non-zero. In the convective instability regime, localized perturbations are driven by the mean flow in such a way that they grow in the moving reference frame, but decay at any fixed location. In contrast, in the absolute instability regime, localized perturbations grow at any fixed location [4]. The behavior of the system is thus qualitatively very different in both the regimes. Such instabilities lead to the formation of various kinds of spatio-temporal patterns [1]. The well-known examples are the rectangular Rayleigh–Bénard convection cell [5], the pattern of thermo-capillary waves in a laterally heated liquid layer [6], the spiral waves in the Couette–Taylor flow between counter-rotating cylinders [7], the traveling inclined vortex flow in the Taylor–Dean system [8] and the electro hydrodynamic instabilities in the nematic liquid crystal [9]. The above models also permitted us to observe experimentally coherent structures such as fronts, pulses, defects and holes [10–12]. Localized defects or holes have been shown to play an important role in the

spatio-temporal intermittency regime [13–16]. The properties of spatio-temporal intermittency states (turbulent bursts and spiral turbulence) in the counter-rotating Couette–Taylor system have been investigated experimentally [15]. The spatio-temporal intermittency regime has also been observed in extended systems such as Rayleigh–Bénard convection [17].

Research was conducted in the case of open flows and in bounded containers: in the case of homogeneous boundary conditions [4, 18, 19], in the periodic boundary conditions [13, 14, 20–27], in the Neumann boundary conditions [22, 28] and also in the case of homogeneous and Neumann boundary conditions [29]. These boundary conditions have an influence on the stability of the system and pattern generation. Deissler [30] used the boundary conditions $A(L,t)=0$ and $A_{xx}(0,t)=0$ to mimic an open flow at $x=0$. Nana *et al* [18] used the boundary conditions $A(0,t)=A(L,t)=0$ to illustrate the variety of novel behaviors that occur when unidirectional waves interact with boundaries. Descalzi and Brand [19] investigated the influence of Dirichlet boundary conditions on various types of localized solutions of the cubic–quintic complex Ginzburg–Landau equation (CGLE) as it arises as an envelope equation near the weakly inverted onset of traveling waves. They found that various types of non-moving pulses and holes can accommodate Dirichlet boundary conditions by having, for holes, two halves of a π hole at each end of the box. They showed that moving pulses of fixed shape as they arise for periodic boundary conditions are replaced by a non-moving asymmetric pulse, which has half a π hole at the end of the box in the original moving direction to guarantee that Dirichlet boundary conditions are met. In their work, Houghton *et al* [28] used the boundary conditions $A_x(0)=A_x(L)=0$ to investigate the CGLE with drift on a finite domain and they examined the simultaneous effects of drift and boundaries on the bistable Benjamin–Feir stable regime.

Colet *et al* [31] used the boundary conditions $A(0)=A_x(L)=0$ to study the nature of the instability of the homogeneous steady states of the subcritical real Ginzburg–Landau equation in the presence of the group velocity. They considered systems described by this equation and analyzed some problems related to the effect of group velocities on the stability of its steady states.

In recent work [21], we studied the behavior of the traveling waves in an extended system by using periodic boundary conditions. We found many different types of spatio-temporal regimes such as phase turbulence, weak turbulence, spatio-temporal intermittency and defect turbulence. Couairon and Chomaz [32] investigated the pushed global modes in weakly inhomogeneous subcritical flows. They showed that the nonlinear global modes satisfy a boundary condition accounting for the inlet of the flow. They also demonstrated that, in a large region of parameters, the nonlinear global mode has the same spatial structure as in the real case and oscillates at the global frequency selected at threshold by the pushed front. In other domains, as for example in optic fibers, the cubic–quintic CGLE has also been used to study the modulational instability in an extended system [33].

The goal of this work is to study the one-dimensional (1D) wave patterns described by the cubic–quintic CGLE in the finite domain, in which the amplitude of the wave pattern vanishes at the lateral boundaries of the domain: to retrieve numerically some coherent structures observed experimentally, in the case of absolute or convective instabilities. The first stage is devoted to the building of a front between the trivial state and the bifurcating one. It is during the second stage that this front moves outwards or inwards according to the convective or absolute nature of the instability. With the perturbation of wave patterns, the domain can remain stable or chaotic depending on the level of perturbation, and coherent structures (holes, defects) are observed.

The outline of this paper is as follows. In section 2, we present the 1D cubic–quintic CGLE. In section 3, we give an analytical approach of the model equation. In section 4, we build a state of phase diagram in the parameter plane spanned by the bifurcation parameter and the quintic nonlinear coefficient. We study the spatio-temporal evolution of the wave patterns, and show that depending on the values of the quintic nonlinear term c_5, many structures are observed in the domain. Finally, the conclusion is given in section 5.

2. The cubic–quintic complex Ginzburg–Landau equation

We consider the cubic–quintic CGLE which may be derived, for example, by weakly nonlinear analysis of the Taylor–Couette system or Rayleigh–Bénard convection with throughflow [34, 35]. The 1D cubic–quintic CGLE is given by

$$\frac{\partial A}{\partial t}=\nu\frac{\partial A}{\partial x}+(1+\mathrm{i}c_1)\frac{\partial^2 A}{\partial x^2}+\mu A+(1-\mathrm{i}c_3)|A|^2A - (1-\mathrm{i}c_5)|A|^4A,\quad 0\leqslant x\leqslant L, \tag{1}$$

where $A(x,t)$ is the complex wave patterns amplitude. This equation describes the envelope of a traveling wave propagating at the group velocity ν toward negative x and is controlled by six parameters: c_1, c_3, c_5, ν, μ and L [32, 33, 36]. The wave is driven by real coefficients c_1, c_3 and c_5, which describe linear dispersion and nonlinear frequencies detuning, respectively; μ is the criticality parameter and L is the length of the domain [36]. The coefficient c_1 is assumed to be positive since equation (1) possesses the symmetry $(A\to\bar{A},\ c_1\to -c_1)$, where the overbar denotes complex conjugation [3].

We are interested in flows evolving in bounded geometries with a finite domain, in which the amplitude of the wave patterns vanishes at the lateral boundaries of the domain [7, 8, 37, 38]. We have chosen these boundary conditions in accordance with experimental data from the thermo-convective experiment with a horizontal temperature gradient [6], or on Couette–Taylor flows [7, 38], in the Taylor–Dean system [9], and in von Karman vortex shedding for circular cylinders [10, 11]. In these experiments, the amplitude of disturbance tends to zero near lateral boundaries.

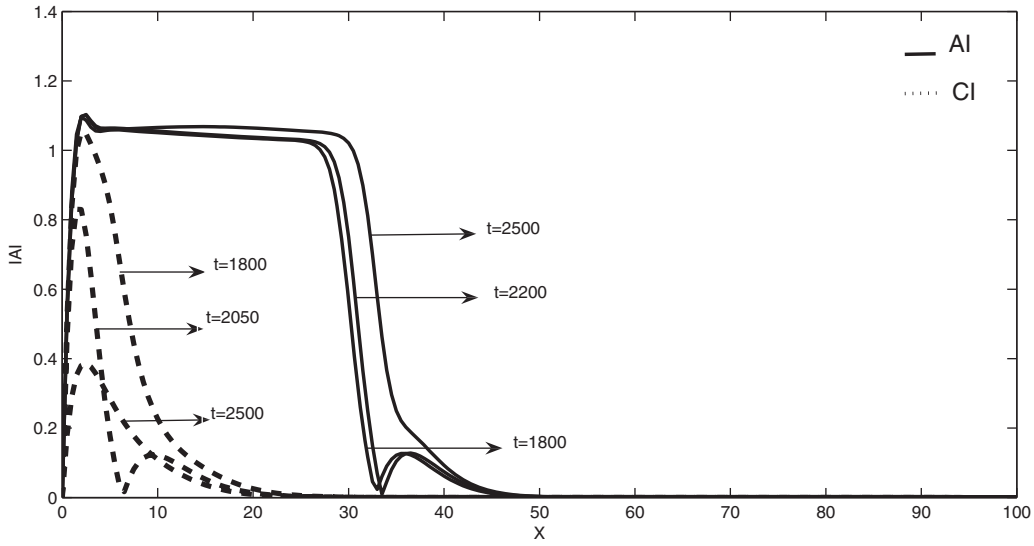

Figure 1. Profiles of the amplitude of an initial perturbation at different times for $\nu = 1.0$, $c_1 = 0.45$, $c_3 = 2.0$, $c_5 = 2.0$ and $L = 100$: in the convective instability (CI) regime with $\mu = 0.15$ (dashed lines) and in the absolute instability (AI) regime with $\mu = 0.3$ (solid lines).

The homogeneous boundary conditions are given by

$$A(x = 0, t) = A(x = L, t) = 0. \tag{2}$$

The size of the domain L is fixed by the experiment while it takes discrete values for periodic boundary conditions. It should be noted that the existence of finite boundaries breaks the space translational invariance, so it is not possible to eliminate the group velocity v by a transformation to a moving frame of reference. Therefore, the 1D system described by the cubic–quintic CGLE is spanned by five parameter spaces: μ, ν, c_1, c_3 and c_5.

Equation (1) admits the trivial solution $A = 0$ and spatially homogeneous solutions of finite amplitude:

$$A = A_0\, \mathrm{e}^{\mathrm{i}\omega t}, \quad |A_0|^2 = \frac{1}{2}(1 \pm \sqrt{4\mu + 1}), \tag{3}$$

with $\omega = -c_3|A_0|^2 + c_5|A_0|^4$ and where the (+) sign in the bracket of equation (3) corresponds to the physical branch, whereas the (−) sign is associated with the unphysical branch. We describe the theory for the cubic–quintic CGLE for which an analytical understanding of secondary instability is possible.

3. Stability of wave patterns of the 1D cubic–quintic CGLE

3.1. Linear stability analysis

For the evolution of infinitely small perturbations, we shall refer to the linear absolute instability theory initially developed in the context of plasma physics [39]. The spatial homogeneous equation, linearized about the stable state $A = 0$, admits a normal mode of the form $A(x, t) = |A_0| \exp[\mathrm{i}(\Omega t + kx)]$ with the dispersion relation

$$\Omega = \omega_0 + (c_1 - \mathrm{i})(k - k_0)^2. \tag{4}$$

The associated spatial solution $k(\Omega)$ has a branch point at those values (ω_0, k_0) where the group velocity vanishes. The branch point values are

$$\begin{aligned} \omega_0 &= -\frac{\nu^2 c_1}{4(1 + c_1^2)} + \mathrm{i}\left(\mu - \frac{\nu^2}{4(1 + c_1^2)}\right), \\ k_0 &= -\frac{\nu(\mathrm{i} + c_1)}{2(1 + c_1^2)}. \end{aligned} \tag{5}$$

When a particular frame, the 'laboratory frame', is singled out by forcing at a specific location or by the boundary conditions, the above stability considerations should be complemented with the concepts of absolute and convective instability, which quantify the competition between dispersion induced by the instability and basic advection [32]. The nature of the local instability is specified by the sign of the imaginary parts of ω_0 ($\mathrm{Im}\,\omega_0$). The instability is of absolute type when $\mathrm{Im}\,\omega_0 > 0$, which occurs, for fixed values of ν and c_1, when $\mu > \mu_\mathrm{a} = \frac{\nu^2}{4(1+c_1^2)}$. The instability is convective when $0 < \mu < \mu_\mathrm{a}$. It is illustrated by figure 1. This figure shows the deterministic evolution of the wave pattern amplitude for convective and absolute instability regimes. When μ varies, the nature of the instability can change with spatial position. Stated in another way, a sustained resonance occurs when the region of absolute instability attains a sufficient size. A nominal criterion for the onset of global dynamical behavior is that the integral of the absolute growth rate ($\sqrt{\mathrm{Im}\,\omega_0}$) over the region where it is positive must be of order one. A linear growth analysis of equation (1) in unbounded domains [1] shows that the far front separating the base state ($A = 0$) and the bifurcated state ($A \neq 0$) moves with velocity

$$v_\mathrm{f} = 2\left[\mu\left(1 + c_1^2\right)\right]^{\frac{1}{2}} - \nu. \tag{6}$$

Then in the convectively unstable regime v_f is negative ($v_\mathrm{f} < 0$), it is positive ($v_\mathrm{f} > 0$) in the absolute instability regime and zero at $\mu = \mu_\mathrm{a}$; for this last value the front is stationary.

Let us note that, in the convective regime, the localized disturbances of the basic state are growing but step away from the source. This is why we have restricted the study to

the dynamics of pattern for parameters corresponding to the absolute instability regime. For convenience in our work, we consider that the parameters ν, c_1, c_3 are fixed and we have varied the parameters μ and c_5. To validate our work, we have used the analytical results for absolute and convective instability for the parameters of a linear equation, and by choosing the values $c_1 = 0.45$ and $\nu = 1.0$, the transition from convective to absolute instability occurs at $\mu_a = 0.207$ [4]. In order to agree with some experimental data obtained in the absolute case by using the CGLE, we have chosen to fix $c_3 = 2.0$ [4].

3.2. Stability of nonlinear traveling waves

When the criticality parameter μ increases, the linear stability fails and the waves can involve new localized structures. The periodic basic solution loses its stability, a secondary instability appears and we can observe new states in the domain. As a result, the frequency Ω close to $x = L$ differs from Ω_f (Ω_f is the value of the frequency of the front) and has to be determined numerically, even for $L \gg 1$. This leads to a nonlinear eigenvalue problem for Ω whose solution depends both on μ and on the details of the boundary conditions applied at $x = L$. The dependence of the frequency Ω on μ, and the instability of the periodic solution to a secondary front can only be investigated systematically by resolving the nonlinear eigenvalue problem [4, 28]. We have assumed that the solution of equation (1) is given by

$$A = \mathrm{e}^{\mathrm{i}\Omega t}(A_0(x) + \varepsilon A_1(x)\,\mathrm{e}^{\mathrm{i}\omega t + \mathrm{st}} + \varepsilon A_2^*(x)\,\mathrm{e}^{-\mathrm{i}\omega t + \mathrm{st}}), \quad \varepsilon \ll 1. \tag{7}$$

Here $A_0(x)$ is the basic periodic solution oscillating with frequency Ω. $A_1(x)$ and $A_2(x)$ are linear, periodic perturbations with a different frequency ω and the growth rate s. Substituting solution (7) into equation (1) we obtained

$$\mathrm{i}\Omega A_0 = \nu A_{0x} + \mu A_0 + (1 - \mathrm{i}c_3)|A_0|^2 A_0 - (1 - \mathrm{i}c_5)|A_0|^4 A_0 + (1 + \mathrm{i}c_1)A_{0xx} \tag{8}$$

and

$$\begin{aligned}(s + \mathrm{i}(\omega + \Omega))A_1 &= \nu A_{1x} + \mu A_1 + (1 - \mathrm{i}c_3)(2|A_0|^2 A_1 + A_0^2 A_2) \\ &-(1 - \mathrm{i}c_5)(2|A_0|^2 A_0^2 A_2 + 3|A_0|^4 A_1) + (1 + \mathrm{i}c_1)A_{1xx}, \\ (s + \mathrm{i}(-\omega + \Omega))A_2 &= \nu A_{2x} + \mu A_2 + (1 - \mathrm{i}c_3)(2|A_0|^2 A_2^* + A_0^2 A_1^*) \\ &-(1 - \mathrm{i}c_5)(2|A_0|^2 A_0^2 A_1^* + 3|A_0|^4 A_2^*) + (1 + \mathrm{i}c_1)A_{2xx}^*\end{aligned} \tag{9}$$

with the boundary conditions

$$\begin{aligned}&A_0(0) = A_0(L) = 0 \quad \text{and} \\ &A_1(0) = A_2(0) = A_1(L) = A_2(L) = 0.\end{aligned} \tag{10}$$

Thus, the system of equations (8) and (9) with boundary conditions (10) constitutes a two-point boundary value problem for the complex functions A_0, A_1 and A_2. The three eigenvalues Ω, s and ω have been found by fixing the gradients of the functions A_0, A_1 and A_2 at the boundary $x = 0$. We have solved this boundary value problem by using the Matlab code function bvp4c [40]. In fact, equation (8) can be solved separately, and by fixing the parameters c_1, c_3, c_5 and ν, we have found the variation of the eigenvalue Ω as a function of the criticality parameter μ, together with the corresponding function $A_0(x)$. The basic periodic solution is unstable to the formation of the secondary solution as is seen in figure 2. This instability occurs when the growth rate s of the linear perturbation becomes positive. Figure 2 shows that the linear periodic perturbation A_1 has the form of the wall mode pressed against the left boundary, with a clearly defined wave number. This situation could be explained as follows. If one gives to the control parameter μ a value greater than a critical value μ_c, secondary structures will appear at the left boundary of the system. In this case, depending on the sign of the nonlinear dispersion coefficient, secondary structures were excited from a regular wave pattern [18]. It must be recognized that the value of μ_c depends also on the size of the system: if the system is large, the more the value of μ_c. So, a system with small size is more sensitive to such a linear, periodic perturbation.

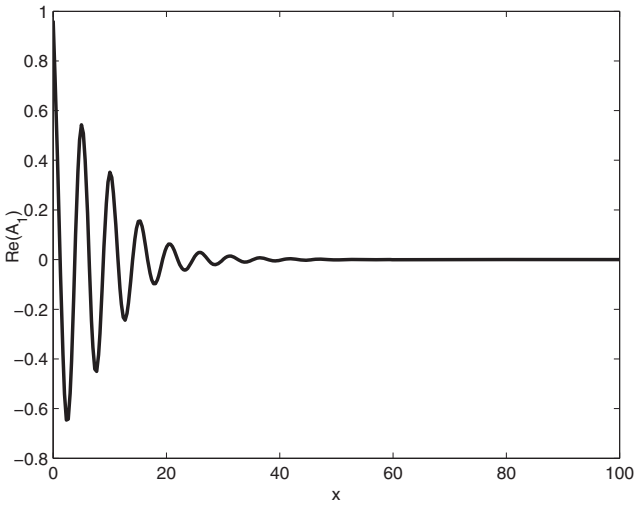

Figure 2. Graph of $\mathrm{Re}(A_1)$ for $\mu = 1.4$, $c_1 = 0.450$, $c_3 = 2.0$, $c_5 = 2.0$, $L = 100$, $\Omega = 1.2$ and $\nu = 1$.

4. Numerical simulations of the 1D cubic–quintic CGLE

Our aim in this section is to study the dynamics of the spatio-temporal traveling waves in bounded containers. The predictions of the Ginzburg–Landau model presented in section 3 were evaluated numerically. Equation (1) (with boundary conditions (equation (2)) was integrated with a fully explicit finite difference scheme and a fourth-order Runge–Kutta time step [18, 21]. The discrete form of the Dirichlet boundary condition that we use is $A_1 = A_n = 0$. The precision of the numerical results is examined by testing several steps of integration in space and in time. We have chosen a grid spacing $\mathrm{d}x = 0.5$ and the typical time step was $\mathrm{d}t = 0.055$. Typically, we consider a system involving N sites with $N = 201$ points. The simulation was started from an approximation of a pulse-like solution with a low amplitude [18, 19]. We investigate the effects of the quintic nonlinear coefficient c_5 in equation (1) with the homogeneous Dirichlet boundary conditions. Then we fix c_1,

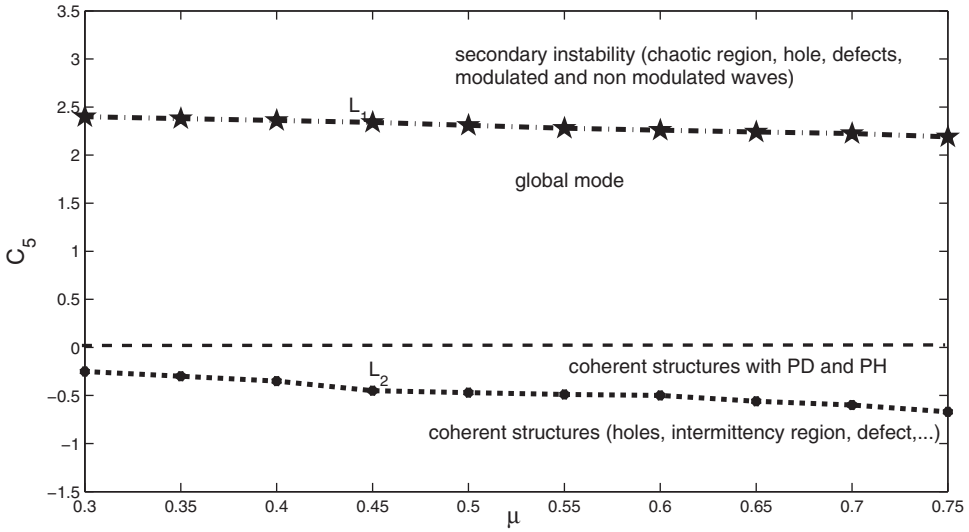

Figure 3. Phase diagram in (μ, c_5), with $c_1 = 0.45$, $c_3 = 2.0$, $\nu = 1$ and $L = 100$: PD and PH stand for periodic defects and periodic holes regions, respectively.

c_3, ν, L and we vary μ and c_5. This variation enabled us to identify, in the parameter space (μ, c_5), zones in which the wave patterns exhibit different behaviors. Solving the 1D cubic–quintic CGLE for several values of c_5 in the absolute instability regime leads to bifurcation of the global mode to new states that are summarized in the phase diagram of figure 3 for $c_5 \in [-1.5; 3.5]$. It is important to note that, in our numerical simulations, the system is practically insensitive to the variation of c_5 in the convective instability regime. No global mode is observed. We have found that the threshold of convective–absolute instability is $\mu_a = 0.207$. Our phase diagram is obtained only in the absolute instability regime ($\mu \geqslant \mu_a$). Let us recall that the subcritical bifurcation is saturated to quintic order. This is why we focus our investigations on the quintic term c_5 with the criticality parameter μ.

For the quintic nonlinear coefficient c_5 positive, we have the line L_1 of figure 3 which separates two zones: the global mode from the secondary instability. Below the line L_1, the global mode is stable and above it, the global mode pertains to a secondary instability that leads to different types of wave patterns. The secondary structures are created by the secondary front which is close to the downstream boundary. The global mode under the line L_1 is represented by figure 4. This figure 4 demonstrates the selection of the stable waves in the global mode. It reveals that the wave patterns are decreasing in time and propagate in only one direction toward the left.

Now, we study the behavior of the wave patterns above the line L_1. The variation of the coefficient c_5 leads to bifurcation of the global mode to new states, which is illustrated in figure 5, for $c_5 = 2.4$ and $\mu = 0.65$. This figure shows the nature of the transitions that can occur. This plot reveals that the solution can break up into several disjoint states with different properties separated by more fronts defined by the location of the states. For this value of c_5, all the plane waves lose their stability and small perturbations bring the system to a spatio-temporally disordered cellular

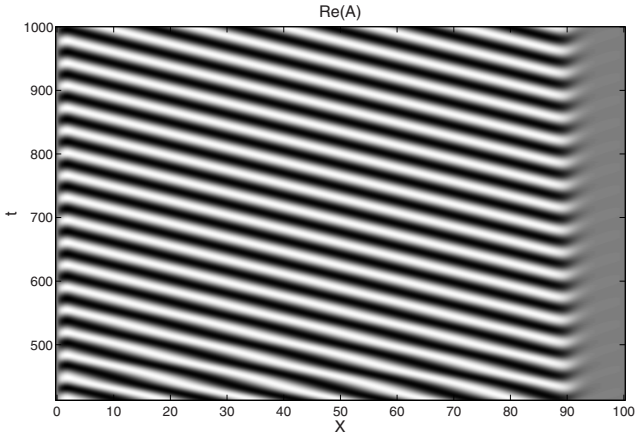

Figure 4. Space–time variation of the Re(A) for $\mu = 0.3$, $c_1 = 0.450$, $c_3 = 2.0$, $c_5 = 2.0$, $L = 100$ and $\nu = 1$, showing global modes.

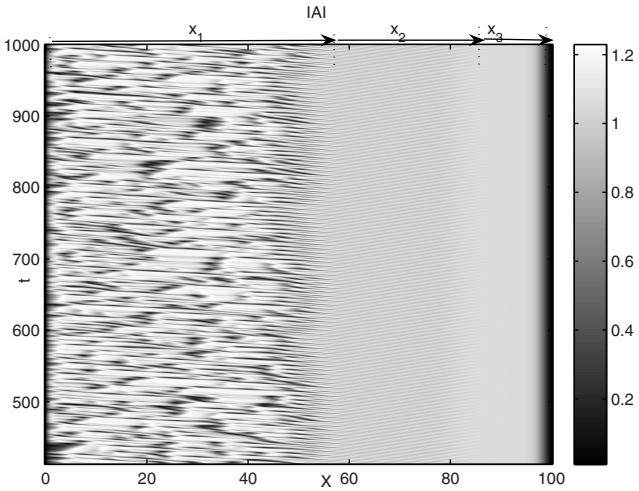

Figure 5. Space–time variation of the wave pattern amplitude $|A|$, for $\mu = 0.65$, $c_1 = 0.450$, $c_3 = 2.0$, $c_5 = 2.37$, $L = 100$ and $\nu = 1$, indicating the appearance of the secondary structures.

state. The regular pattern is destabilized and gives rise to a spatio-temporal turbulent state near the wall $x = 0$ (space x_1) which is separated by a modulated state in space and time, where we have the modulated patterns (space x_2) while, near the end $x = L$, the wave pattern remains non-modulated and the regular wave train is observed (space x_3). The wave patterns are formed as a result of several successive absolute secondary instabilities, each of which is responsible for the introduction of a new front into the structure of the solution, as described in [28, 41]. In [6], the authors have reported an experimental study of the secondary modulational instability of a 1D nonlinear traveling wave in a long bounded channel. They identified two qualitatively different instability regimes involving fronts of spatio-temporal defects. They focused on the distinction between the convective and the absolute modulational instability regimes and the relevance of similar structures: a front of dislocations or modulation. The chaotic and non-modulated spaces are also separated to the boundaries by the fronts. The presence of the defect and holes is detected in the chaotic space. Defects and holes are local structures that play a crucial role in the intermediate regime between laminar states and hard chaos. Defects are points in the space–time diagram where the amplitude of the wave vanishes and the phase is not defined. In two and higher dimensions, such defects can disappear only via collisions with other defects, and act as long-living seeds for local structures like spirals [42]. The holes are characterized by a local concentration of the phase gradient and a depression of the wave amplitude $|A|$ (hence the name 'hole'). The one-parameter family of traveling hole solutions discovered by Nozaki and Bekki [43] has been shown to play an important dynamical role in a large portion of parameter space, including in a region where they are linearly unstable [14]. Similar objects have been identified in various experimental contexts of *a priori* relevance, e.g. Rayleigh–Bénard convection, coupled wakes [12, 37] and in Couette–Taylor flow [38].

We have noticed that when c_5 further increases, the chaotic region propagates into the domain toward the upstream boundary and the system becomes more and more chaotic. The non-modulated and modulated states undergo propagation of the chaotic state, they are advected also toward $x = L$ and decrease in space.

For negative values of c_5, the entire domain is secondarily unstable and destabilized differently. Then, the coherent structures are observed. The domain exhibits amplitude defects, holes and a spatio-temporal intermittency regime. It is important to note that in the cubic case, for certain negative values of the nonlinear coefficient, a region of global mode was shown [18]. Figure 6 sketched for $\mu = 0.35$, $c_5 = -0.2$ reveals that the wave patterns are stable at the first part of the domain until the three quarters of the domain and the system still regular. Near the upstream boundary, new structures are revealed (hole, defects, etc). The defects appear at regular time intervals around $x = 80$ and for this reason we call them time-periodic defects (PD). The periodic topological defects have been observed, for example, in many experiments such as fluid convection [44], Taylor–Dean flow [8], in a model for the selection of vortex roll-up patterns in finite aspect ratio, two-dimensional wakes at low to moderate Reynolds

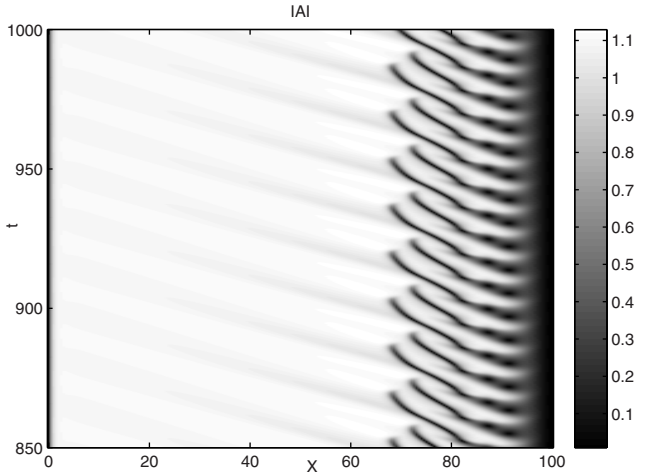

Figure 6. Space–time variation of the $|A|$, for $\mu = 0.35$, $c_1 = 0.450$, $c_3 = 2.0$, $c_5 = -0.2$, $L = 100$ and $\nu = 1$, denoting coherence structure with PD and PH.

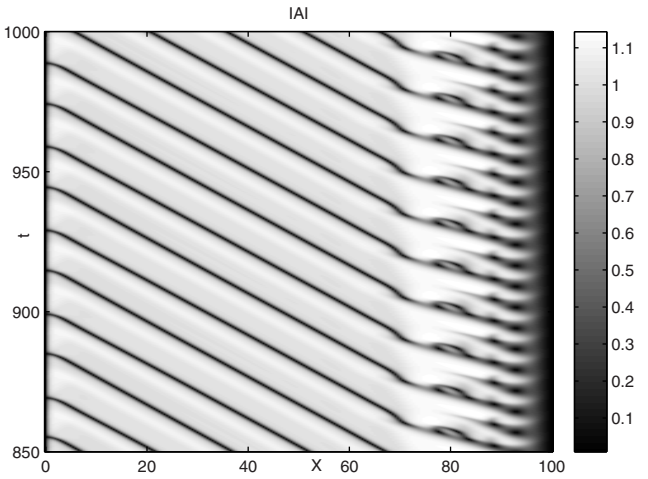

Figure 7. Space–time variation of the wave pattern amplitude $|A|$ showing also coherence structures with PD and PH, for $\mu = 0.3$, $c_1 = 0.450$, $c_3 = 2.0$, $c_5 = -0.25$, $L = 100$ and $\nu = 1$.

number [13]. Near the right boundary, holes are observed and also before the PD, around $x = 70$. Holes that appear near the upstream boundary are regular in a time interval and we call them periodic holes (PH). Figure 7 is obtained for $\mu = 0.40$ and $c_5 = -0.25$. This figure reveals that the nucleation of the phase jumps near $x = L$ occurs periodically with a well-defined period. It exposes a periodic sequence of phase jumps propagating in the advection direction (i.e. to the left), and the wave pattern amplitude is modulated in this region. We notice that defects are advected toward the upstream boundary and the core of the defect is localized around $x = 88$ (PD). Holes are detected around $x = 92$ and are periodic in a time interval (PH). One notes that there are more holes in the domain, which means one can observe more or less point holes if the values of control parameters μ and c_5 are varied. Figure 8 is obtained when the wave patterns are below the line L_2 for $\mu = 0.3$ and $c_5 = -0.6$. This space–time reveals the disordered regimes in the domain and the behavior of the patterns becomes more complex. The figure reveals the presence of the core of defects around $x = 85$ which are

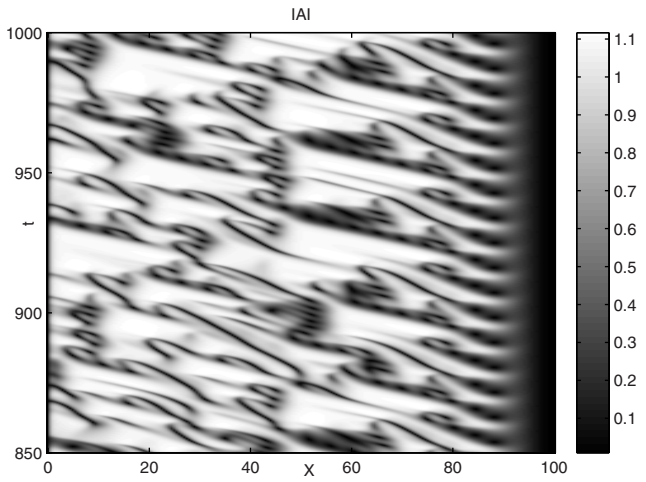

Figure 8. Space–time variation of the wave pattern amplitude $|A|$, for $\mu = 0.3$, $c_1 = 0.450$, $c_3 = 2.0$, $c_5 = -0.6$, $L = 100$ and $\nu = 1$, displaying spatio-temporal intermittency, defects, holes.

periodic. Before the PD, a disordered regime is observed. This disordered regime is a spatio-temporal intermittency regime [13].

5. Conclusion

In this paper, we have described from the 1D cubic–quintic CGLE the effects of the boundaries on the waves traveling in a preferred direction. We have used the homogeneous boundary conditions and the waves were nonlinear dissipative waves. In the considered cubic–quintic CGLE, the dynamics of the wave patterns were controlled by six parameters. In the light of explaining some experimental visualization, we fixed the length of the domain, the group velocity, the linear dispersion coefficient and the cubic nonlinear dispersion coefficient while we varied the criticality parameter and the quintic nonlinear dispersion coefficient. We studied the nature of convective or absolute instabilities of wave patterns. In our simulations, we found new structures which, to our knowledge, have not been observed in numerical simulations of the 1D CGLE. Only results of the experiments present similar structures [5, 6, 8, 10, 11, 38]. The presence of the quintic term has a large influence on the wave pattern. We have shown that, depending on the sign of the quintic nonlinear coefficient, regular wave patterns, amplitude modulated, holes and defects were observed.

In the case of positive values of the quintic nonlinear coefficient c_5, we have seen that the dispersion is normal; in contrast, it is the opposite in the cubic case where the dispersion is anomalous [4, 18]. Beyond a certain value of c_5, the domain becomes chaotic and the presence of defects and holes has been observed. For negative values of c_5, we have shown that all of the system is secondarily unstable and we found new wave patterns that exhibit holes with or without temporal periodic amplitude defects, depending on the values of c_5. The presence of the intermittency regime in the wave patterns has also been observed. The stability analysis of the basic wave train for $c_5 < 0$ is beyond the impact of this work. Such defects, holes and spatio-temporal intermittency regimes have been observed in the spiral wave pattern in the counter-rotating Couette–Taylor system [7], in the Taylor–Dean system [8] and in Rayleigh–Bénard convection [5]. These results were different from those that used periodic boundary conditions [13, 14, 21, 22]. They are also different from those that used homogeneous boundary conditions [19]. The difference observed between the results of our work and those of [19] is due to the presence of a group velocity term. This term involves the moving of the instability toward the end of the domain. The numerical investigation of the 1D cubic–quintic CGLE with homogeneous boundary conditions for different values of the control parameters represents an important topic in understanding many physical systems with pattern formation.

Acknowledgment

The authors would like to thank Professor I Mutabazi of the University of Havre (France) for fruitful discussions during this work.

References

[1] Cross M C and Hohenberg P C 1993 *Rev. Mod. Phys.* **65** 851
[2] Walgraef D 1996 *Spatio-Temporal Pattern Formation with Examples in Physics Chemistry and Materials Science* (New York: Springer)
[3] Couairon A and Chomaz J M 1999 *Physica* D **132** 428
[4] Tobias S M, Proctor M R E and Knobloch E 1998 *Physica* D **113** 43
[5] Kolodner P, Walder R W, Passner A and Surko C M J 1986 *Fluid Mech.* **163** 195
[6] Garnier N, Chiffaudel A and Daviaud F 2002 *Phys. Rev. Lett.* **88** 134501
[7] Nana L, Ezersky A B, Abcha N and Mutabazi I 2008 *J. Phys.: Conf. Ser.* **137** 012006
[8] Bot P and Mutabazi I 2000 *Eur. Phys. J.* B **13** 141
[9] Joets A and Ribotta R 1988 *Propagation in Systems Far from Equilibrium* ed J E Wesfreid *et al* (New York: Springer) p 176
[10] Park D S and Redekopp L G 1992 *Phys. Fluids* **4** 1697
[11] Monkewitz P A, Williamson C H K and Miller G D 1996 *Phys. Fluids* **8** 91
[12] Albarède P and Monkewitz P A 1992 *Phys. Fluids* A **4** 744
[13] Chaté H 1994 *Nonlinearity* **7** 185
[14] Van Hecke M 1998 *Phys. Rev. Lett.* **80** 1896
[15] Goharzadeh A and Mutabazi I 2001 *Eur. Phys. J.* B **19** 157
[16] Hayot F and Pomeau Y 1994 *Phys. Rev.* E **50** 2019
[17] Daviaud F, Bonetti M and Dubois M 1990 *Phys. Rev.* A **42** 3388
[18] Nana L, Ezersky A B and Mutabazi I 2009 *Proc. R. Soc. Lond.* A **465** 2251
[19] Descalzi O and Brand H R 2010 *Phys. Rev.* E **81** 026210
[20] Howard M and Van Hecke M 2003 *Phys. Rev.* E **68** 026213
[21] Gonpe Tafo J B, Nana L and Kofane T C 2011 *Eur. Phys. J. Plus* **126** 105
[22] Descalzi O and Brand H R 2008 *Prog. Theor. Phys.* **119** 725
[23] Descalzi O, Argentina M and Tirapegui E 2003 *Phys. Rev.* E **67** 015601
[24] Van Saarloos W and Hohenberg P C 1990 *Phys. Rev. Lett.* **64** 749
[25] Descalzi O, Escaff J C D and Brand H R 2009 *Phys. Rev. Lett.* **102** 188302
[26] Descalzi O 2005 *Phys. Rev.* E **72** 046210
[27] Cartes C, Descalzi O and Brand H R 2012 *Phys. Rev.* E **85** 015205

[28] Houghton S M, Tobias S M, Knobloch E and Proctor M R E 2009 *Physica* D **238** 184
[29] Eguiluz M V, Hernandez-Garcia E and Piro O 2001 *Phys. Rev.* E **64** 036205
[30] Deissler R J 1985 *Stat. Phys.* **40** 371
[31] Colet P, San Miguel M and Walgraef D 1999 *Eur. Phys. J.* B **11** 517
[32] Couairon A and Chomaz J M 2001 *Physica* D **158** 129
[33] Kenfack Jiotsa A and Kofane T C J 2003 *Phys. Soc. Japan* **72** 1800
[34] Büchel P, Lücke M, Roth D and Schmitz R 1996 *Phys. Rev.* E **53** 4764
[35] Müller H W, Lücke M and Kamps M 1992 *Phys. Rev.* A **45** 3714
[36] Aranson I S and Kramer L 2002 *Rev. Mod. Phys.* **74** 99
[37] Ezersky A B, Kiyashko S V and Nazarovsky A V 2001 *Physica* D **152** 310
[38] Lepiller V, Goharzadeh A, Prigent A and Mutabazi I 2008 *Eur. Phys. J.* B **61** 445
[39] Lifshitz E M and Pitaevskii L P 1981 *Physical Kinetics* (London: Pergamon)
[40] Shampine L F, Gladwell I and Thompson S 2003 *Solving ODEs with Matlab* (New York: Cambridge University Press)
[41] Boccaletti S and Bragard J 2006 *Phil. Trans. R. Soc.* A **364** 2383
[42] Aranson I S, Aranson L, Kramer L and Weber A 1992 *Phys. Rev.* A **46** R2992
[43] Bekki N and Nozaki K 1985 *Phys. Lett.* A **110** 133
[44] Voss H U, Kolodner P, Abel M and Kurths J 1999 *Phys. Rev. Lett.* **83** 3422